

# Spintronics and Quantum Dots for Quantum Computing and Quantum Communication

Guido Burkard, Hans-Andreas Engel, and Daniel Loss  
*Department of Physics and Astronomy, University of Basel,  
Klingelbergstrasse 82, CH-4056 Basel, Switzerland*  
(April 11, 2000)

Control over electron-spin states, such as coherent manipulation, filtering and measurement promises access to new technologies in conventional as well as in quantum computation and quantum communication. We review our proposal of using electron spins in quantum confined structures as qubits and discuss the requirements for implementing a quantum computer. We describe several realizations of one- and two-qubit gates and of the read-in and read-out tasks. We discuss recently proposed schemes for using a single quantum dot as spin-filter and spin-memory device. Considering electronic EPR pairs needed for quantum communication we show that their spin entanglement can be detected in mesoscopic transport measurements using metallic as well as superconducting leads attached to the dots.

## I. INTRODUCTION

\* Theoretical research on electronic properties in mesoscopic condensed matter systems has focussed primarily on the charge degrees of freedom of the electron, while its spin degrees of freedom have not yet received the same attention. However, an increasing number of spin-related experiments [1–6] show that the spin of the electron offers unique possibilities for finding novel mechanisms for information processing and information transmission—most notably in quantum-confined nanostructures with unusually long spin dephasing times [2–4] approaching microseconds, as well as long distances of up to  $100\mu\text{m}$  [2] over which spins can be transported phase-coherently. Besides the intrinsic interest in spin-related phenomena, there are two main areas which hold promises for future applications: Spin-based devices in conventional [1] as well as in quantum computer hardware [7]. In conventional computers, the electron spin can be expected to enhance the performance of quantum electronic devices, examples being spin-transistors (based on spin-currents and spin injection), non-volatile memories, single spin as the ultimate limit of information storage etc. [1]. On the one hand, none of these devices exist yet, and experimental progress as well as theoretical investigations are needed to provide guidance and support in the search for realizable implementations. On the other hand, the emerging field of quantum computing [8,9] and quantum communication [9,10] requires a radically new approach to the design of the necessary hardware. As first pointed out in Ref. [7], the spin of the electron is a most natural candidate for the qubit—the fundamental unit of quantum information. We have shown [7] that these spin qubits, when located in quantum-confined struc-

tures such as semiconductor quantum dots or atoms or molecules, satisfy all requirements needed for a scalable quantum computer. Moreover, such spin-qubits—being attached to an electron with orbital degrees of freedom—can be transported along conducting wires between different subunits in a quantum network [9]. In particular, spin-entangled electrons can be created in coupled quantum dots and—as mobile Einstein-Podolsky-Rosen (EPR) pairs [9]—provide then the necessary resources for quantum communication.

For both spin-related areas—conventional computers and quantum computers—similar and sometimes identical physical concepts and tools are needed, the common short-term goal being to find ways to control the coherent dynamics of electron spins in quantum-confined nanostructures. It is this common goal that makes research on the electron spin in nanostructures—spintronics—a highly attractive area. While we advance our basic knowledge about spin physics in many-body systems, we gain insights that promise to be useful for future technologies.

We have remarked earlier [11] that there have been almost as many proposals for solid state implementations of quantum computers as all the other proposals put together. A clear reason for this is that solid state physics is a most versatile branch of physics, in that almost any phenomenon possible in physics can be embodied in an appropriately designed condensed matter system. A related reason is that solid state physics, being so closely allied with computer technology, has exhibited great versatility in the creation of artificial structures and devices. This has been exploited to produce ever more capable computational devices. It appears natural to expect that this versatility will extend to the creation of solid state

---

\*Prepared for Fortschritte der Physik special issue,  
*Experimental Proposals for Quantum Computation*,  
eds. H.-K. Lo and S. Braunstein.

quantum computers as well; the plethora of proposals would indicate that this is indeed true, although only time can tell whether any of these proposals will actually provide a successful route to a quantum computer.

In the following we will review the current status of our theoretical efforts towards the goal of implementing quantum computation and quantum communication with electron spins in quantum-confined nanostructures. Most of the results presented here have been discussed at various places in the literature to which we refer the interested reader for more details.

### A. Quantum Computing and Quantum Communication

The long-term goal of our investigations is quantum information processing with electron spins. Thus, a brief description of this emerging research field and its goals are in order. Quantum computing has attracted much interest recently as it opens up the possibility of outperforming classical computation through new and more powerful quantum algorithms such as the ones discovered by Shor [12] and by Grover [13]. There is now a growing list of quantum tasks [9,10] such as cryptography, error correcting schemes, quantum teleportation, etc. that have indicated even more the desirability of experimental implementations of quantum computing. In a quantum computer each quantum bit (qubit) is allowed to be in any state of a quantum two-level system. All quantum algorithms can be implemented by concatenating one- and two-qubit gates. There is a growing num-

ber of proposed physical implementations of qubits and quantum gates. A few examples are: Trapped ions [14], cavity QED [15], nuclear spins [16,17], superconducting devices [18–21], and our qubit proposal [7] based on the spin of the electron in quantum-confined nanostructures.

Coupled quantum dots provide a powerful source of deterministic entanglement between qubits of localized but also of delocalized electrons [9,7]. E.g., with such quantum gates it is possible to create a singlet state out of two electrons and subsequently separate (by electronic transport) the two electrons spatially with the spins of the two electrons still being entangled—the prototype of an EPR pair. This opens up the possibility to study a new class of quantum phenomena in electronic nanostructures [9] such as the entanglement and non-locality of electronic EPR pairs, tests of Bell inequalities, quantum teleportation [22], and quantum cryptography [23] which promises secure information transmission.

### B. Quantum Dots

In the present work, quantum dots play a central role and thus we shall make some general remarks about these systems here. Semiconductor quantum dots are structures where charge carriers are confined in all three spatial dimensions, the dot size being of the order of the Fermi wavelength in the host material, typically between 10nm and 1 $\mu$ m [24]. The confinement is usually achieved by electrical gating of a two-dimensional electron gas (2DEG), possibly combined with etching techniques, see Fig. 1. Precise control of the number of electrons in the

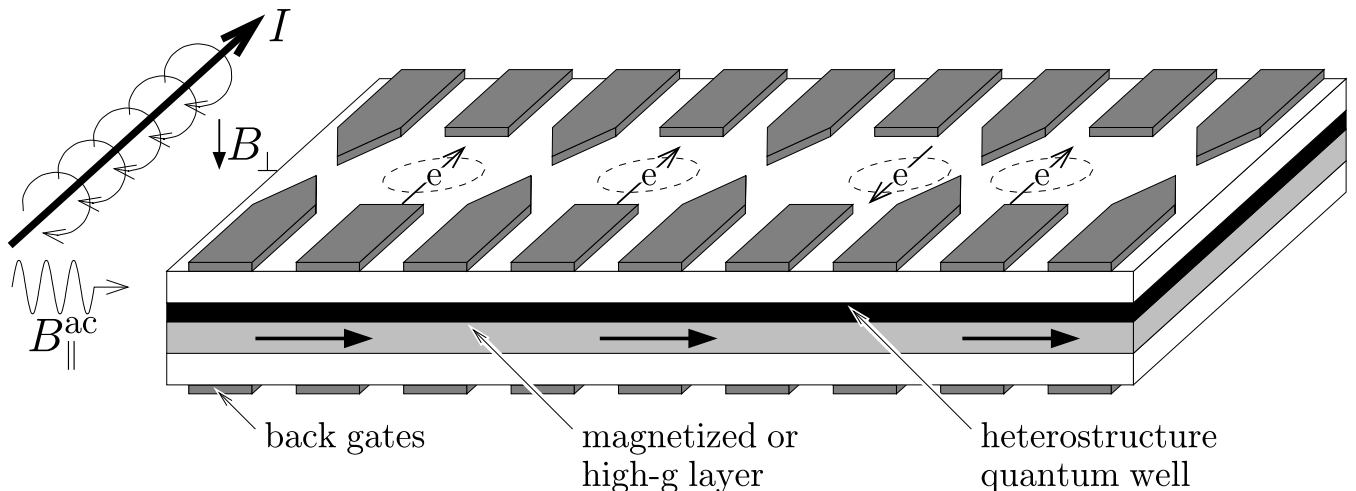


FIG. 1. An all-electrically controlled quantum dot array. The electrodes (dark gray) confine single electrons to the dot regions (circles). The electrons can be moved by electrical gating into the magnetized or high- $g$  layer to produce locally different Zeeman splittings. Alternatively, such local Zeeman fields can be produced by magnetic field gradients as e.g. produced by a current wire (indicated on the left of the dot-array). Since every dot-spin is subject to a different Zeeman splitting, the spins can be addressed individually, e.g. through ESR pulses of an additional in-plane magnetic ac field with the corresponding Larmor frequency  $\omega_L$ . Such mechanisms can be used for single-spin rotations and the initialization step (see Sec. IIH and Sec. IV). The exchange coupling between the dots is controlled by electrically lowering the tunnel barrier between the dots, see Sec. IIIA. In this figure, the two rightmost dots are drawn schematically as tunnel-coupled.

conduction band of a quantum dot (starting from zero) has been achieved in GaAs heterostructures [25]. The electronic spectrum of typical quantum dots can vary strongly when an external magnetic field is applied [24,25], since the magnetic length corresponding to typical laboratory fields  $B \approx 1$  T is comparable to typical dot sizes. In coupled quantum dots Coulomb blockade effects [26], tunneling between neighboring dots [24,26], and magnetization [27] have been observed as well as the formation of a delocalized single-particle state [28].

## II. GENERAL CONSIDERATIONS FOR QUANTUM COMPUTING WITH SPINS

### A. Coherence

A fundamental problem in quantum physics is the issue of the decoherence of quantum systems and the transition between quantum and classical behavior. Of course, a lot of attention has been devoted in fundamental mesoscopic research to characterizing and understanding the decoherence of electrons in small structures. We remind the reader, however, that most of what has been probed (say in weak localization studies or the Aharonov-Bohm effect) is the *orbital* coherence of electron states, that is, the preservation of the relative phase of superpositions of spatial states of the electron (e.g., in the upper and lower arm of an Aharonov-Bohm ring). The coherence times seen in these investigations are almost completely irrelevant to the *spin* coherence times which are important in our quantum computer proposal. There is some relation between the two if there are strong spin-orbit effects, but our intention is that conditions and materials should be chosen such that these effects are weak.

Under these circumstances the spin coherence times (the time over which the phase of a superposition of spin-up and spin-down states is well-defined) can be completely different from the charge coherence times (a few nanoseconds), and in fact it is known that they can be orders of magnitude longer (see below). This was actually one of our prime motivations for proposing spin [7] rather than charge as the qubit in these structures. The experimental measurement of this kind of coherence (i.e. for spins) is not so familiar in mesoscopic physics, and thus it is worth describing it briefly here.

In recent magneto-optical experiments, based on time-resolved Faraday rotation measurements, long spin coherence times were found in doped GaAs in the bulk and a 2DEG [2]. At vanishing magnetic field and  $T = 5$  K, a transverse spin lifetime (decoherence time)  $T_2^*$  exceeding 100 ns was measured, with experimental indications that this time is a single-spin effect [2]. Since this number still includes inhomogeneous effects—e.g. g-factor variations in the material, leading to spins rotating with slightly different frequencies and thus reducing the total magnetization—it represents only a lower bound of

the transverse lifetime of a *single* spin,  $T_2 \geq T_2^*$ , which is relevant for using spins as qubits. Using the same pump-probe technique, spin lifetimes in semiconductor quantum dots have been measured [29], with at most one spin per dot. The relatively small  $T_2^*$  decoherence times (a few ns at vanishing magnetic field), which have been seen in these experiments, probably originate from a large inhomogeneous broadening due to a strong variation of g-factors [29]. Nevertheless, the fact that many coherent oscillations were observed [29] provides strong experimental support to the idea of using electron spin as qubits.

Since none of the experiments have been done on an actual quantum computing structure as we envision it (see below), the existing results cannot be viewed as conclusive. Because of sensitivity to details, theory can only give general guidance about the mechanisms and dependencies to be looked for, but cannot make reliable *a priori* predictions of the decoherence times.

In fact there are further complications [7,11]: we know theoretically that decoherence is not actually fully characterized by a single rate; in fact, a whole set of numbers is needed to fully characterize the decoherence process (12 in principle for individual qubits), and no experiment has been set up yet to completely measure this set of parameters, although the theory of these measurements is available. Even worse, decoherence effects will in principle be modified by the act of performing quantum computation (during gate operation, decoherence is occurring in a coupled qubit system [7]). We believe that the full characterization of decoherence will involve ongoing iteration between theory and experiment, and will thus be inseparable from the act of building a reliable quantum computer. Still, we should mention that recent calculations [30] including spin-orbit interaction lead to unusually low phonon-assisted spin-flip rates in quantum dots, which indicates long spin-decoherence times. We will discuss spin-qubit errors due to nuclear spins [31] below in Sec. II G.

### B. Upscaling

For the implementation of realistic calculations on a quantum computer, a large number of qubits will be necessary (on the order of  $10^5$ ). For this it is essential that the underlying concept can be scaled up to a large number of qubits, which then can be operated in parallel (parallelism is required in known error correction schemes, see Sec. II E). This scaling requirement is well achievable with spin-based qubits confined in quantum dots, since producing arrays of quantum dots [9,11] is feasible with state-of-the-art techniques of defining nanostructures in semiconductors. Of course, the actual implementation of such arrays including all the needed circuits poses experimental challenges, but at least we are not aware of physical restrictions which would exclude such an upscal-

ing for spin-qubits.

### C. Pulsed Switching

As we discuss in Sec. III and IV, quantum gate operations will be controlled through an effective Hamiltonian

$$H(t) = \sum_{i < j} J_{ij}(t) \mathbf{S}_i \cdot \mathbf{S}_j + \sum_i \mu_B g_i(t) \mathbf{B}_i(t) \cdot \mathbf{S}_i, \quad (1)$$

which is switched via external control fields  $v(t)$ . Note that in the following the exchange coupling is local, i.e.  $J_{ij}$  is finite only for neighboring qubits. However, in cavity-QED systems, there is also a long-range coupling of qubits as some of us have described in Ref. [32]. But even if the exchange coupling is only local, operations on non-neighboring qubits can still be performed. Since one can swap the state of two qubits with the help of the exchange interaction only, as we will show in Sec. III, the qubits can be moved around in an array of quantum dots. Thus, a qubit can be transported to a place where it can be coupled with a desired second qubit, where single-qubit operations can be performed, or where it can be measured.

The gating mechanisms described in Sec. III and IV do not depend on the shape of  $P(v(t))$ , where  $P$  stands for the exchange coupling  $J$  or the Zeeman interaction. Only the time integral  $\int_0^\tau P(v(t))dt$  needs to assume a certain value (modulo  $2\pi$ ). The exchange interaction  $J(t)$  should be switched adiabatically, i.e. such that  $|\dot{v}/v| \ll \delta\varepsilon/\hbar$ , where  $\delta\varepsilon$  is the energy scale on which excitations may occur. Here,  $\delta\varepsilon$  should be taken as the energy-level separation of a single dot (if spin is conserved). A rectangular pulse leads to excitation of higher levels, whereas an adiabatic pulse with amplitude  $v_0$  is e.g. given by  $v(t) = v_0 \operatorname{sech}(t/\Delta t)$  where  $\Delta t$  controls the width of the pulse. We need to use a switching time  $\tau_s > \Delta t$ , such that  $v(t = \tau_s/2)/v_0$  becomes vanishingly small. We then have  $|\dot{v}/v| = |\tanh(t/\Delta t)|/\Delta t \leq 1/\Delta t$ , so we need  $1/\Delta t \ll \delta\varepsilon/\hbar$  for adiabatic switching. The Fourier transform  $v(\omega) = \Delta t v_0 \pi \operatorname{sech}(\pi\omega\Delta t)$  has the same shape as  $v(t)$  but width  $2/\pi\Delta t$ . In particular,  $v(\omega)$  decays exponentially in the frequency  $\omega$ , whereas it decays only with  $1/\omega$  for a rectangular pulse.

### D. Switching Times

Single qubit operations can be performed for example in g-factor-modulated materials, as proposed in Sec. IV. A spin can be rotated by a relative angle of  $\phi = \Delta g_{\text{eff}} \mu_B B \tau / 2\hbar$  through changing the effective g-factor by  $\Delta g_{\text{eff}}$  for a time  $\tau$ . Thus, a typical switching time for an angle  $\phi = \pi/2$ , a field  $B = 1$  T, and  $\Delta g_{\text{eff}} \approx 1$  is  $\tau_s \approx 30$  ps. If slower operations are required, they are easily implemented by choosing a smaller  $\Delta g_{\text{eff}}$ , reducing the magnitude of the field  $B$ , or by replacing  $\phi$

by  $\phi + 2\pi n$  with integer  $n$ , thus “overrotating” the spin. Next we consider two exchange-coupled spins, which perform a square-root-of-swap gate for the integrated pulse  $\int_0^{\tau_s} J(t)dt/\hbar = \pi/2$ , as described in Sec. III. We apply a pulse (see Sec. II C)  $J(t) = J_0 \operatorname{sech}(t/\Delta t)$  with  $J_0 = 80 \mu\text{eV} \approx 1$  K and  $\Delta t = 4$  ps. Again, we calculate a switching time  $\tau_s \approx 30$ ps, while the adiabaticity criterion is  $\hbar/\Delta t \approx 150 \mu\text{eV} \ll \delta\varepsilon$ . Once more, the switching time can be easily increased by adding  $2\pi n$  with integer  $n$  to the integrated pulse  $\int_0^{\tau_s} J(t)/\hbar$ , i.e. by “overswapping” the two spins. This increased switching time allows a slower switching of  $J(t)$  if required.

Further, we note that the total time consumed by an algorithm can be optimized considerably by simultaneously switching different parameters of the Hamiltonian, i.e. producing parallel instead of serial pulses. As an example, we have shown that for an error-correcting algorithm using only three qubits, a speed-up of a factor of two can be achieved [33]. For algorithms handling a larger number of qubits, a more drastic optimization can be expected.

### E. Error Correction

One of the main goals in quantum computation is the realization of a reliable error-correction scheme [34], which requires gate operations with an error rate not larger than one part in  $10^4$ . Taking the ratio of the dephasing time from Sec. II A,  $T_2 \geq 100$  ns, and the switching times from Sec. II D,  $\tau_s \approx 30$  ps, we see that the targeted error rate seems not to be out of reach in the near future. From there on, an arbitrary upscaling of a quantum computer becomes feasible and is no further limited by decoherence and lacking gate precision, at least when systems with a scalable number of qubits are considered. We note that a larger number of qubits also requires a larger total number of gate operations to be performed, in order to implement the error-correction schemes. Therefore it is inevitable to perform these operations in parallel; otherwise the pursued gain in computational power is used up for error correction. Hence, one favors concepts where a localized control of the gates can be realized such that operations can be performed in parallel. However, since there are still many milestones to reach before sophisticated error-correction schemes can be applied, one should by no means disregard setups where gate operations are performed in a serial way.

### F. Precision Requirements

Quantum computation is not only spoiled by decoherence, but also by a limited precision of the gates, i.e. by the limited precision of the Hamiltonian. In order for error correcting schemes to work, the (time integrated) exchange and Zeeman interaction need to be controlled

again in about one part in  $10^4$ . While this requirement is present in all quantum computer proposals, it emphasizes the importance of gates with fine control. After a gate operation was performed on two qubits, one should be able to turn off the coupling between these qubits very efficiently, e.g. exponentially in the external fields, such that errors resulting from the remaining coupling can be reduced efficiently (if there is still a remaining coupling this can easily result in correlated errors; however, such correlated errors would pose new problems since known error correction schemes explicitly exclude them). The exchange coupling between two quantum dots can be indeed suppressed exponentially, as we will describe below in Sec. III. A further possible source of errors are fluctuating charges in the environment (e.g. moving charges in the leads attached to the gates) since they can lead to unknown shifts of the electrostatic potentials raised and lowered for switching. However, it is known from experiments on single quantum dots that such charge fluctuations can be controlled on the scale of hours [35] which is sufficiently long on the time-scale set by the spin decoherence time which can be on the order of  $10^{-6}$  secs. Still, the ability to suppress  $1/f$  noise will be very important for well-controlled switching in quantum computation. Finally, we note that uncontrolled charge switching is not nearly so great a problem for spin qubits as for charge qubits, since this switching does not couple directly to the spin degree of freedom.

### G. Decoherence due to Nuclear Spins

It turns out that a serious source of possible qubit errors using semiconductors such as GaAs is the hyperfine coupling between electron spin (qubit) and nuclear spins in the quantum dot [31]. In GaAs semiconductors, both Ga and As possess a nuclear spin  $I = 3/2$ , and no Ga/As isotopes are available with zero nuclear spin. This is in contrast to Si-based structures which would be more advantageous from this aspect. However, in Si the control over nanostructures such as quantum dots is not as advanced as in GaAs yet, but this might be just a question of time. Anyway, we shall now see that such decoherence effects can also be controlled by creating an Overhauser field [31].

The hyperfine coupling between the electron spin  $\mathbf{S}$  and the nuclear spins  $\mathbf{I} = \sum_{n=1}^N \mathbf{I}^{(n)}$ , is given by  $A \mathbf{S} \cdot \mathbf{I}$ , where  $A$  is the hyperfine coupling constant. Due to this coupling, a flip of the electron spin with a concomitant change of one nuclear spin may occur, causing an error in the quantum computation. We have analyzed this error in the presence of a magnetic field  $B_z$  [31], and find in time-dependent perturbation theory that the total probability for a flip of the electron spin oscillates in time. The amplitude of these oscillations is

$$P_i \approx \frac{1}{N} \left( \frac{B_n^*}{B} \right)^2, \quad (2)$$

where  $B$  is defined below and  $B_n^* = NAI/g\mu_B$  is the maximal magnitude of the effective nuclear field (Overhauser field). In typical quantum dots we have  $N \sim 10^5$ . If  $B_z = 0$  and with a polarization  $p \neq 0$ ,  $-1 \leq p \leq 1$  of the nuclear spins, an effective nuclear field  $B = pB_n^*$  is produced and the transition probability becomes suppressed with  $P_i \approx 1/p^2N$ . Such a polarization  $p$  can be established by dynamically spin-polarizing the nuclear spins, e.g. by optical pumping [36] or by spin-polarized currents at the edge of a 2DEG [37]. For these methods, nuclear Overhauser fields are reported as large as  $pB_n^* = 4$  T in GaAs (corresponding to  $p = 0.85$ ) [37] and which can have a lifetime on the order of minutes [36]. Alternatively, for unpolarized nuclei, the amplitude of  $P_i$  can be suppressed by an external field  $B = B_z$  [Eq. (2)]. Thus, the decoherence of an electron spin due to hyperfine interaction can be suppressed drastically, either by dynamically polarizing the nuclear spins in the host material or by applying an external magnetic field. It would be highly desirable to test this prediction by measuring the electron-spin  $T_2$  time with and without Overhauser field.

### H. Initialization

At the beginning of most algorithms for quantum computers as well as an input for error correcting schemes, initialized qubits are required, i.e. qubits in a well defined state such as spin up,  $|\uparrow\rangle$ . Single spins can be polarized by exposing them to a large magnetic field  $g\mu_B B \gg kT$  and letting them relax to the ground state. Such a magnetic field could be applied locally or realized by forcing the electrons (via external gates) into a magnetized layer, into a layer with a different effective g-factor [7,9] or into a layer with polarized nuclear spins (Overhauser effect) [31] etc., see also Fig. 1 and Sec. IV. If a spin-polarized current can be produced, such as by spin-polarizing materials [3,4] or by spin-filtering with the help of another dot [38] (see Sec. V C), polarized electrons can be injected into an empty quantum dot, i.e. the dot is filled with an already initialized spin.

For some algorithms, it is favorable to start with a given initial state, such as  $|0110\dots\rangle$ , instead of a ground state  $|0000\dots\rangle$ . This can be readily implemented with spins as qubits using standard electron spin resonance (ESR) techniques [31]: We start with a ground state  $|0000\dots\rangle$ . Then we produce a Zeeman splitting by applying a static local magnetic field for these spins, which should be initialized into state  $|1\rangle$ . An ac magnetic field is then applied perpendicularly to the first field with a resonant frequency that matches the Larmor frequency  $\omega_L = g\mu_B B/\hbar$ . Due to paramagnetic resonance [39], this causes spin-flips in the quantum dots with the corresponding Zeeman splitting, thus producing the desired state. We note that since we do not want to affect the

other spins (having a different Zeeman splitting) the amplitude of the ac field must be switched adiabatically, see Sec. II C. Of course, spin precession can also be used to perform single-spin rotations (see Sec. IV).

### III. TWO-QUBIT GATES—COUPLED QUANTUM DOTS

The main component for every computer concept is a multi-(qu)bit gate, which eventually allows calculations through combination of several (qu)bits. Since two-qubit gates are (in combination with single-qubit operations) sufficient for quantum computation [40]—they form a universal set—we now focus on a mechanism that couples pairs of spin-qubits. Such a mechanism exists in coupled quantum dots, resulting from the combined action of the Coulomb interaction and the Pauli exclusion principle. Two coupled electrons in absence of a magnetic field have a spin-singlet ground state, while the first excited state in the presence of strong Coulomb repulsion is a spin triplet. Higher excited states are separated from these two lowest states by an energy gap, given either by the Coulomb repulsion or the single-particle confinement. The low-energy dynamics of such a system can be described by the effective Heisenberg spin Hamiltonian

$$H_s(t) = J(t) \mathbf{S}_1 \cdot \mathbf{S}_2, \quad (3)$$

where  $J(t)$  denotes the exchange coupling between the two spins  $\mathbf{S}_1$  and  $\mathbf{S}_2$ , i.e. the energy difference between the triplet and the singlet. After a pulse of  $J(t)$  with  $\int_0^{\tau_s} dt J(t)/\hbar = J_0 \tau_s/\hbar = \pi \pmod{2\pi}$ , the time evolution  $U(t) = T \exp(i \int_0^t H_s(\tau) d\tau/\hbar)$  corresponds to the “swap” operator  $U_{\text{sw}}$ , whose application leads to an interchange of the states in qubit 1 and 2 [7]. While  $U_{\text{sw}}$  is not sufficient for quantum computation, any of its square roots  $U_{\text{sw}}^{1/2}$ , say  $U_{\text{sw}}^{1/2}|\phi\chi\rangle = (|\phi\chi\rangle + i|\chi\phi\rangle)/(1+i)$ , turns out to be a *universal* quantum gate. Thus, it can be used, together with single-qubit rotations, to assemble any quantum algorithm. This is shown by constructing the known universal gate XOR [41], through combination of  $U_{\text{sw}}^{1/2}$  and single-qubit operations  $\exp(i\pi S_i^z/2)$ , applied in the sequence [7],

$$U_{\text{XOR}} = e^{i(\pi/2)S_1^z} e^{-i(\pi/2)S_2^z} U_{\text{sw}}^{1/2} e^{i\pi S_1^z} U_{\text{sw}}^{1/2}. \quad (4)$$

With these universal gates at hand, we can reduce the study of general quantum computation to the study of single-spin rotations (see Sec. IV) and the *exchange mechanism*, in particular how  $J(t)$  can be controlled experimentally. The central idea is that  $J(t)$  can be switched by raising or lowering the tunneling barrier between the dots. In the following, we shall review our detailed calculations to describe such a mechanism. We note that the same principles can also be applied to other spin systems in quantum-confined structures, such as coupled atoms in a crystal, supramolecular structures,

and overlapping shallow donors in semiconductors [17,42] etc., using similar methods as explained below. We point out that, beyond the mechanisms described in Sec. III A and Sec. III B, spins in quantum dots can also be coupled on a long distance scale by using a cavity-QED scheme [32] or by using superconducting leads to which the quantum dots are attached [43], see Sec. VI D.

#### A. Laterally Coupled Dots

We consider a system of two coupled quantum dots in a two-dimensional electron gas (2DEG), containing one (excess) electron each, as described in Sec. I B. The dots are arranged in a plane, at a sufficiently small distance  $2a$ , such that the electrons can tunnel between the dots (for a lowered barrier) and an exchange interaction  $J$  between the two spins is produced. We model this system of coupled dots with the Hamiltonian  $H = \sum_{i=1,2} h_i + C + H_Z = H_{\text{orb}} + H_Z$ , where the single-electron dynamics in the 2DEG ( $xy$ -plane) is described through

$$h_i = \frac{1}{2m} \left( \mathbf{p}_i - \frac{e}{c} \mathbf{A}(\mathbf{r}_i) \right)^2 + V(\mathbf{r}_i), \quad (5)$$

with  $m$  being the effective mass and  $V(\mathbf{r}_i)$  the confinement potential as given below. A magnetic field  $\mathbf{B} = (0, 0, B)$  is applied along the  $z$ -axis, which couples to the electron spin through the Zeeman interaction  $H_Z$  and to the charge through the vector potential  $\mathbf{A}(\mathbf{r}) = \frac{B}{2}(-y, x, 0)$ . In almost depleted regions, like few-electron quantum dots, the screening length  $\lambda$  can be expected to be much larger than the screening length in bulk 2DEG regions (where it is 40 nm for GaAs). Thus, for small quantum dots, say  $\lambda \gg 2a \approx 40$  nm, we need to consider the bare Coulomb interaction  $C = e^2/\kappa|\mathbf{r}_1 - \mathbf{r}_2|$ , where  $\kappa$  is the static dielectric constant. The confinement and tunnel-coupling in Eq. (5) for laterally aligned dots is modeled by the quartic potential

$$V(x, y) = \frac{m\omega_0^2}{2} \left[ \frac{1}{4a^2} (x^2 - a^2)^2 + y^2 \right], \quad (6)$$

with the inter-dot distance  $2a$  and  $a_B = \sqrt{\hbar/m\omega_0}$  the effective Bohr radius of the dot. Separated dots ( $a \gg a_B$ ) are thus modeled as two harmonic wells with frequency  $\omega_0$ . This is motivated by the experimental evidence that the low-energy spectrum of single dots is well described by a parabolic confinement potential [25].

Now we consider only the two lowest orbital eigenstates of  $H_{\text{orb}}$ , leaving us with one symmetric (spin-singlet) and one antisymmetric (spin-triplet) orbital state. The spin state for the singlet is  $|S\rangle = (|\uparrow\downarrow\rangle - |\downarrow\uparrow\rangle)/\sqrt{2}$ , while the triplet spin states are  $|T_0\rangle = (|\uparrow\downarrow\rangle + |\downarrow\uparrow\rangle)/\sqrt{2}$ ,  $|T_+\rangle = |\uparrow\uparrow\rangle$ , and  $|T_-\rangle = |\downarrow\downarrow\rangle$ . For temperatures with  $kT \ll \hbar\omega_0$ , higher-lying states are frozen out and  $H_{\text{orb}}$  can be replaced by the effective Heisenberg spin Hamiltonian

[Eq. (3)]. The exchange energy  $J = \epsilon_t - \epsilon_s$  is given as the difference between the triplet and singlet energy. For calculating these energies, we use the analogy between atoms and quantum dots and make use of variational methods similar to the ones in molecular physics. Using the Heitler-London ansatz with ground-state single-dot orbitals, we find [31],

$$J = \frac{\hbar\omega_0}{\sinh(2d^2 \frac{2b-1}{b})} \left\{ \frac{3}{4b} (1 + bd^2) + c\sqrt{b} \left[ e^{-bd^2} I_0(bd^2) - e^{d^2(b-1)/b} I_0\left(d^2 \frac{b-1}{b}\right) \right] \right\}, \quad (7)$$

where we have introduced the dimensionless distance  $d = a/a_B$  between the dots and the magnetic compression factor  $b = B/B_0 = \sqrt{1 + \omega_L^2/\omega_0^2}$  with the Larmor frequency  $\omega_L = eB/2mc$ . The zeroth order Bessel function is denoted by  $I_0$ . In Eq. (7), the first term comes from the confinement potential, while the terms proportional to the parameter  $c = \sqrt{\pi}/2(e^2/\kappa a_B)/\hbar\omega_0$  result from the Coulomb interaction  $C$ ; the exchange term is recognized by its negative sign. We are mainly interested in the weak coupling limit  $|J/\hbar\omega_0| \ll 1$ , where the ground-state Heitler-London ansatz is self-consistent. We plot  $J$  [Eq. (7)] in Fig. 2 as a function of  $B$  and  $d$ . We note that  $J(B=0) > 0$ , which is generally true for a two-particle system with time-reversal invariance. We observe that over a wide range of the parameters  $c$  and  $a$ , the sign of  $J(B)$  changes from positive to negative at a finite value of  $B$  (for the parameters chosen in Fig. 2(a) at  $B \approx 1.3$  T).  $J$  is suppressed exponentially either by compression of the electron orbitals through large magnetic fields ( $b \gg 1$ ), or by large distances between the dots ( $d \gg 1$ ), where in both cases the orbital overlap of the two dots is reduced. This exponential suppression, contained in the  $1/\sinh$  prefactor in Eq. (7), is partly compensated by the exponentially growing exchange term  $\propto \exp(2d^2(b-1/b))$ . In total,  $J$  decays exponentially as  $\exp(-2d^2b)$  for large  $b$  or  $d$ . Since the sign reversal of  $J$ —signalling a singlet-triplet crossing—results from the long-range Coulomb interaction, it is not contained in the standard Hubbard model which takes only short-range interaction into account. In this latter model one finds  $J = 4t^2/U > 0$  in the limit  $t/U \ll 1$  (see Fig. 2). The Heitler-London result [Eq. (7)] was refined by taking higher levels and double occupancy of the dots into account (implemented in a Hund-Mullikan approach), which leads to qualitatively similar results [31], in particular concerning the singlet-triplet crossing.

We remark again that the exponential suppression of  $J$  is very desirable for minimizing gate errors, see Sec. II F. In the absence of tunneling between the dots we still might have direct Coulomb interaction left between the electrons. However, this has no effect on the spins (qubit) provided the spin-orbit coupling is sufficiently small, which is the case for s-wave electrons in GaAs structures with unbroken inversion symmetry (this

would not be so for hole-doped systems since the hole has a much stronger spin-orbit coupling due to its p-wave character). Finally, the vanishing of  $J$  can be exploited for switching by applying a constant homogeneous magnetic field to an array of quantum dots to tune  $J$  to zero (or close to some other desirable value). Then, for switching  $J$  on and off, only a small gate pulse or a small local magnetic field is needed.

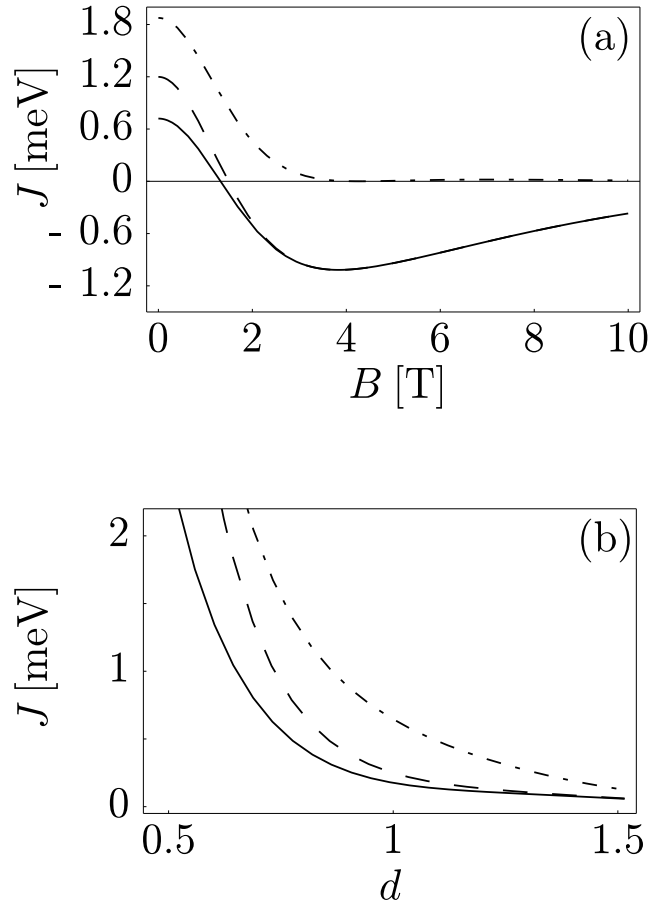


FIG. 2. Exchange coupling  $J$  (full line) for GaAs quantum dots with confinement energy  $\hbar\omega = 3$  meV and  $c = 2.42$ . For comparison we plot the usual short-range Hubbard result  $J = 4t^2/U$  (dashed-dotted line) and the extended Hubbard result [31]  $J = 4t^2/U + V$  (dashed line). In (a),  $J$  is plotted as a function of the magnetic field  $B$  at fixed inter-dot distance  $d = a/a_B = 0.7$ , while in (b) as a function of the inter-dot distance  $d = a/a_B$  at  $B = 0$ .

## B. Vertically Coupled Dots

We have also investigated the case of vertically tunnel-coupled quantum dots [44]. Such a setup of the dots has been produced in multilayer self-assembled quantum dots (SAD) [45] as well as in etched mesa heterostructures [46]. We apply the same methods as described in Sec. III A for laterally coupled dots, but now we extend

the Hamiltonian Eq. (5) from two to three dimensions and take a three-dimensional confinement  $V = V_l + V_v$ . We implement the vertical confinement  $V_v$  as a quartic potential similar to Eq. (6), with curvature  $\omega_z$  at  $z = \pm a$  [see Fig. 3(b)], implying an effective Bohr radius  $a_B = \sqrt{\hbar/m\omega_z}$  and a dimensionless distance  $d = a/a_B$ . We have modeled a harmonic potential for the lateral confinement, while we have allowed different sizes of the two dots  $a_{B\pm} = \sqrt{\hbar/m\alpha_{0\pm}\omega_z}$ . This allows additional switching mechanisms as it is explained in the next paragraph.

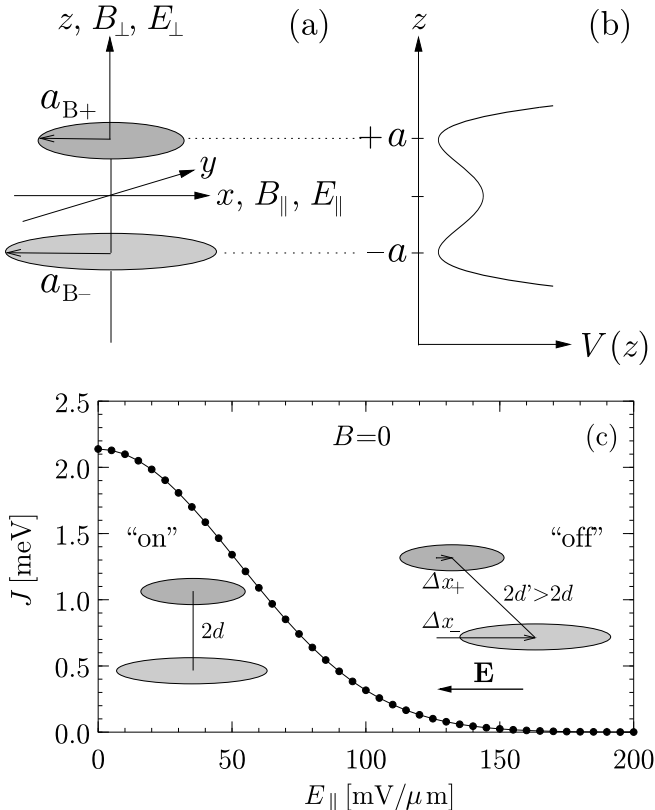


FIG. 3. (a) Two vertically coupled quantum dots with different lateral diameters  $a_{B+}$  and  $a_{B-}$ . In the text, we discuss magnetic and electric fields applied either in-plane ( $B_{\parallel}$ ,  $E_{\parallel}$ ) or perpendicularly ( $B_{\perp}$ ,  $E_{\perp}$ ). (b) The quartic double-well potential used for modeling the vertical confinement  $V_v$ , see text. (c) Switching of the spin-spin coupling between dots of different size by means of an in-plane electric field  $E_{\parallel}$  at  $B=0$ . We have chosen  $\hbar\omega_z = 7$  meV,  $d = 1$ ,  $\alpha_{0+} = 1/2$  and  $\alpha_{0-} = 1/4$ . For these parameters,  $E_0 = \hbar\omega_z/ea_B = 0.56$  mV/nm and  $A = (\alpha_{0+}^2 - \alpha_{0-}^2)/2\alpha_{0+}^2\alpha_{0-}^2 = 6$ . The exchange coupling  $J$  decreases exponentially on the scale  $E_0/2A = 47$  mV/ $\mu$ m for the electric field. Thus, the exchange coupling is switched “on” for  $E_{\parallel} = 0$  and “off” for  $E_{\parallel} \gtrsim 150$  mV/ $\mu$ m, see text.

Since we are considering a three-dimensional setup, the exchange interaction is not only sensitive to the magnitude of the applied fields, but also to their direction. We now give a brief overview of our results [44] for in-plane ( $B_{\parallel}$ ,  $E_{\parallel}$ ) and perpendicular ( $B_{\perp}$ ,  $E_{\perp}$ ) fields; this

setup is illustrated in Fig. 3(a): (1) An in-plane magnetic field  $B_{\parallel}$  suppresses  $J$  exponentially; a perpendicular field in laterally coupled dots has the same effect (Sec. III A). (2) A perpendicular magnetic fields  $B_{\perp}$  reduces on the one hand the exchange coupling between identically sized dots  $\alpha_{0+} = \alpha_{0-}$  only slightly. On the other hand, for different dot sizes  $a_{B+} < a_{B-}$ , the behavior of  $J(B_{\perp})$  is no longer monotonic: Increasing  $B_{\perp}$  from zero amplifies the exchange coupling  $J$  until both electronic orbitals are magnetically compressed to approximately the same size, i.e.  $B \approx 2m\alpha_{0+}\omega_z c/e$ . From this point,  $J$  decreases weakly, as for identically sized dots. (3) A perpendicular electric field  $E_{\perp}$  detunes the single-dot levels, and thus reduces the exchange coupling; the very same finding was made for laterally coupled dots and an in-plane electric field [31]. (4) An in-plane electric field  $E_{\parallel}$  and different dot sizes provide another switching mechanism for  $J$ . The dots are shifted parallel to the field by  $\Delta x_{\pm} = E_{\parallel}/E_0\alpha_{0\pm}^2$ , where  $E_0 = \hbar\omega_z/ea_B$ . Thus, the larger dot is shifted a greater distance  $\Delta x_- > \Delta x_+$  and so the mean distance between the electrons grows as  $d' = \sqrt{d^2 + A^2(E_{\parallel}/E_0)^2} > d$ , taking  $A = (\alpha_{0+}^2 - \alpha_{0-}^2)/2\alpha_{0+}^2\alpha_{0-}^2$ . Since the exchange coupling  $J$  is exponentially sensitive to the inter-dot distance  $d'$ , it is suppressed exponentially when an in-plane electric field is applied,  $J \approx \exp[-2A^2(E_{\parallel}/E_0)^2]$ , which is illustrated in Fig. 3(c). Thereby we have given an exponential switching mechanism for quantum gate operation relying only on a tunable electrical field, in addition to the magnetically driven switching discussed above.

### C. Singlet-Triplet Entangling Gate

An operation which encodes a single spin  $1/2$  state  $|\alpha\rangle$  into a singlet or triplet state can be used for measuring the state of the qubit represented by  $|\alpha\rangle$ , when a measurement device capable of distinguishing singlet/triplet states is available (see e.g. Sec. VI C). Further, such an operation acts as an “entangler” for electron pairs used in quantum communication (see Sec. VI). Indeed, we can construct such a two-qubit operation explicitly. While quantum dot 1 is in state  $|\alpha\rangle$ , we prepare the state of the quantum dot 2 to  $|\uparrow\rangle$ , perform a  $U_{sw}^{1/2}$  gate and finally apply a local Zeeman term, generating the time evolution  $\exp\{i(\pi/2)S_1^z\}$ , thus

$$\left. \begin{array}{l} |\uparrow\uparrow\rangle \\ |\downarrow\downarrow\rangle \end{array} \right\} \xrightarrow{e^{i\frac{\pi}{2}S_1^z}U_{sw}^{1/2}} \left\{ \begin{array}{l} e^{i\frac{\pi}{4}}|\uparrow\uparrow\rangle, \\ -i(|\downarrow\downarrow\rangle - |\uparrow\downarrow\rangle)/\sqrt{2}. \end{array} \right. \quad (8)$$

In other words, this operation maps the triplet  $|\uparrow\uparrow\rangle$  (and  $|\downarrow\downarrow\rangle$ ) into itself, while the state  $|\downarrow\uparrow\rangle$  is mapped into the singlet (and  $|\uparrow\downarrow\rangle$  into the triplet  $(|\uparrow\downarrow\rangle + |\downarrow\uparrow\rangle)/\sqrt{2}$ ), up to phase factors.

## IV. SINGLE-SPIN ROTATIONS

A requirement for quantum computing is the possibility to perform one-qubit operations, which translates in the context of spins into single-spin rotations. So it must be possible to expose a specific qubit to a time-varying Zeeman coupling  $(g\mu_B \mathbf{S} \cdot \mathbf{B})(t)$  [31], which can be controlled through both the magnetic field  $\mathbf{B}$  and/or the g-factor  $g$ . Since only phases have a relevance, it is sufficient to rotate all spins of the system at once (e.g. by an external field  $B$ ), but with a different Larmor frequency. We have proposed a number of possible implementations [7,31,9,11] for spin-rotations:

The equilibrium position of the electron can be moved around through electrical gating. Thus, if the electron wave function is pushed into a region with a different magnetic field strength or (effective) g-factor, one produces a relative rotation around the direction of  $\mathbf{B}$  by an angle of  $\phi = (g'B' - gB)\mu_B\tau/2\hbar$ , see Fig. 1. Regions with an increased magnetic field can be provided by a magnetic (dot) material while an effective magnetic field can be produced e.g. with dynamically polarized nuclear spins (Overhauser effect) [31].

We shall now explain a concept for using g-factor-modulated materials [9,11]. In bulk semiconductors the free-electron value of the Landé g-factor  $g_0 = 2.0023$  is modified by spin-orbit coupling. Similarly, the g-factor can be drastically enhanced by doping the semiconductor with magnetic impurities [4,3]. In confined structures such as quantum wells, wires, and dots, the g-factor is further modified and becomes sensitive to an external bias voltage [47]. We have numerically analyzed a system with a layered structure (AlGaAs-GaAs-InAlGaAs-AlGaAs), in which the effective g-factor of electrons is varied by shifting their equilibrium position from one layer to another by electrical gating [48]. We have found that in this structure the effective g-factor can be changed by about  $\Delta g_{\text{eff}} \approx 1$  [11].

Alternatively, one can use ESR techniques for switching (as already explained in Sec. II H).

Furthermore, localized magnetic fields can be generated with the magnetic tip of a scanning force microscope, a magnetic disk writing head, by placing the dots above a grid of current-carrying wires, or by placing a small wire coil above the dot etc.

## V. MEASURING A SINGLE SPIN (READ-OUT)

### A. Spin Measurements through Spontaneous Magnetization

One scheme for reading out the spin of an electron on a quantum dot is implemented by tunneling of this electron into a supercooled paramagnetic dot [7,9]. There the spin induces a magnetization nucleation from the

paramagnetic metastable phase into a ferromagnetic domain, whose magnetization direction  $(\theta, \phi)$  is along the measured spin direction and which can be measured by conventional means. Since this direction is continuous rather than only one of two values, we describe this generalized measurement in the formalism of positive-operator-valued (POV) measurements [49] as projection into the overcomplete set of spin-1/2 coherent states  $|\theta, \phi\rangle = \cos(\theta/2)|\uparrow\rangle + e^{i\phi}\sin(\theta/2)|\downarrow\rangle$ . Thus if we interpret a magnetization direction in the upper hemisphere as  $|\uparrow\rangle$ , we have a 75%-reliable measurement, since  $(1/2\pi)\int_{\theta \geq \pi/2} d\Omega |\langle \uparrow | \theta, \phi \rangle|^2 = 3/4$ , using the normalization constant  $2\pi$  for the coherent spin states.

### B. Spin Measurements via the Charge

While spins have the intrinsic advantage of long decoherence times, it is very hard to measure a single spin directly via its magnetic moment. However, measuring the charge of single electrons is state of the art. Thus it is desirable to have a mechanism for detecting the spin of an electron via measuring charge, i.e. voltage or current [7].

A straightforward concept yielding a potentially 100% reliable measurement requires a switchable “spin-filter” tunnel barrier which allows only, say, spin-up but no spin-down electrons to tunnel. When the measurement of a spin in a quantum dot is to be performed, tunneling between this dot and a second dot, connected to an electrometer, is switched on, but only spin-up electrons are allowed to pass (spin-filtering). Thus if the spin had been up, a charge would be detected in the second dot by the electrometer [7], and no charge otherwise. Again, this is a POV type of measurement (see above). It is known how to build electrometers with single-charge detection capabilities; resolutions down to  $10^{-8}$  of one electron charge have been reported [50]. Spin filtering and also spin-state measurements can be achieved by tunneling through a quantum dot [38] as we shall discuss next.

### C. Quantum Dot as Spin Filter and Read-Out/Memory Device

We discuss now a setup—quantum dot attached to in- and outgoing current leads  $l = 1, 2$ —which can be operated as a spin filter, or as a read-out device, or as a spin-memory where a single spin stores the information [38].

A new feature of this proposal is that the spin-degeneracy is lifted with *different* Zeeman splittings in the dot and in the leads, e.g. by using materials with different effective g-factors for leads and dot [38]. This results in Coulomb blockade peaks and spin-polarized currents which are uniquely associated with the spin state on the dot.

The setup is described by a standard tunneling Hamiltonian  $H_0 + H_T$  [51], where  $H_0 = H_L + H_D$  describes the leads and the dot.  $H_D$  includes the charging and interaction energies of the electrons in the dot as well as their Zeeman energy  $\pm g\mu_B B/2$  in an external magnetic field  $\mathbf{B}$ . The tunneling between leads and the dot is described by  $H_T = \sum_{l,k,p,s} t_{lp} c_{lks}^\dagger d_{ps} + \text{h.c.}$ , where  $c_{lks}$  annihilates electrons with spin  $s$  and momentum  $k$  in lead  $l$  and  $d_{ps}$  annihilates electrons in the dot. We consider the Coulomb blockade regime [24] where the charge on the dot is quantized. Then we apply a standard master-equation approach [52,38] with a reduced density matrix of the dot and calculate the transition rates in a “golden-rule” approach up to 2nd order in  $H_T$ . The first-order contribution to the current is the sequential tunneling current  $I_s$  [24], where the number of electrons on the dot fluctuates and thus the processes of an electron tunneling from the lead onto the dot and vice versa are allowed by energy conservation. The second-order contribution is the cotunneling current  $I_c$  [53], involving a virtual intermediate state with a different number of electrons on the dot (see also Sec. VI C).

We now consider a system, where the Zeeman splitting in the leads is negligible (i.e. much smaller than the Fermi energy) while on the dot it is given as  $\Delta_z = \mu_B |gB|$ . We assume a small bias  $\Delta\mu = \mu_1 - \mu_2 > 0$  between the leads at chemical potential  $\mu_{1,2}$  and low temperatures so that  $\Delta\mu, kT < \delta$ , where  $\delta$  is the characteristic energy-level distance on the dot. First we consider a quantum dot in the ground state, filled with an odd number of electrons with total spin 1/2, which we assume to be  $|\uparrow\rangle$  and to have energy  $E_\uparrow = 0$ . If an electron tunnels from the lead onto the dot, a spin singlet is formed with energy  $E_S$ , while the spin triplets are (usually) excited states with energies  $E_{T_\pm}$  and  $E_{T_0}$ . At the sequential tunneling resonance,  $\mu_1 > E_S > \mu_2$ , where the number of electrons on the dot fluctuates between  $N$  and  $N + 1$ , and in the regime  $E_{T_+} - E_S, \Delta_z > \Delta\mu, kT$ , energy conservation only allows ground state transitions. Thus, spin-up electrons are not allowed to tunnel from lead 1 via the dot into lead 2, since this would involve virtual states  $|T_+\rangle$  and  $|\downarrow\rangle$ , and so we have  $I_s(\uparrow) = 0$  for sequential tunneling. However, spin down electrons may pass through the dot in the process  $\downarrow(\uparrow)_i \rightarrow (\uparrow\downarrow)_f$ , followed by  $(\uparrow\downarrow)_i \rightarrow (\uparrow)\downarrow_f$ . Here the state of the quantum dot is drawn inside the circle, while the states in the leads are drawn to the left and right, *resp.*, of the circle. This leads to a *spin-polarized* sequential tunneling current  $I_s = I_s(\downarrow)$ , which we have calculated as [38]

$$I_s(\downarrow)/I_0 = \theta(\mu_1 - E_S) - \theta(\mu_2 - E_S), \quad k_B T < \Delta\mu, \quad (9)$$

$$I_s(\downarrow)/I_0 = \frac{\Delta\mu}{4k_B T} \cosh^{-2} \left[ \frac{E_S - \mu}{2k_B T} \right], \quad k_B T > \Delta\mu, \quad (10)$$

where  $\mu = (\mu_1 + \mu_2)/2$  and  $I_0 = e\gamma_1\gamma_2/(\gamma_1 + \gamma_2)$ . Here  $\gamma_l = 2\pi\nu |A_{lnn'}|^2$  is the tunneling rate between lead  $l$  and the dot and we have introduced the matrix elements  $A_{ln'n} = \sum_{ps} t_{lp} \langle n' | d_{ps} | n \rangle$ . Similarly, for  $N$  even we find

$I_s(\downarrow) = 0$  while for  $I_s(\uparrow)$  a similar result holds [38] as in Eqs. (9), (10).

Even though  $I_s$  is completely spin-polarized, a leakage of current with opposite polarization arises through cotunneling processes [38]; still the leakage is small, and the efficiency for  $\Delta_z < |E_{T_+} - E_S|$  for spin filtering in the sequential regime becomes [38]

$$I_s(\downarrow)/I_c(\uparrow) \sim \frac{\Delta_z^2}{(\gamma_1 + \gamma_2) \max\{k_B T, \Delta\mu\}}, \quad (11)$$

and equivalently for  $I_s(\uparrow)/I_c(\downarrow)$  at the even-to-odd transition. In the sequential regime we have  $\gamma_i < k_B T, \Delta\mu$ , thus, for  $k_B T, \Delta\mu < \Delta_z$ , we see that the spin-filtering is very efficient.

We discuss now the opposite case where the leads are fully spin polarized with a much smaller Zeeman splitting on the dot [38]. Such a situation can be realized with magnetic semiconductors (with effective g-factors reaching 100 [3]) where spin-injection into GaAs has recently been demonstrated for the first time [3,4]. Another possibility would be to work in the quantum Hall regime where spin-polarized edge states are coupled to a quantum dot [54]. In this setup the device can be used as read-out for the spin state on the dot. Assume now that the spin polarization in both leads is up, and the ground state of the dot contains an odd number of electrons with total spin 1/2. Now the leads can provide and absorb only spin-up electrons. Thus, a sequential tunneling current will only be possible if the dot state is  $|\downarrow\rangle$  (to form a singlet with the incoming electron, whereas the triplet is excluded by energy conservation). Hence, the current is much larger for the spin on the dot being in  $|\downarrow\rangle$  than it is for  $|\uparrow\rangle$ . Again, there is a small cotunneling leakage current for the dot-state  $|\uparrow\rangle$ , with a ratio of the two currents given by Eq. (11). Thus, we can probe (read out) the spin-state on the quantum dot by measuring the current which passes through the dot. Given that the sequential tunneling current is typically on the order of 0.1 – 1 nA [24], we can estimate the read-out frequency  $I/2\pi e$  to be on the order of 0.1 – 1 GHz. Combining this with the initialization and read-in techniques from Sec. II H, i.e. ESR pulses to switch the spin state, we have a *spin memory* at the ultimate single-spin limit, whose relaxation time is just the spin relaxation time. This relaxation time can be expected to be on the order of 100’s of nanoseconds [2], and can be directly measured via the currents when they switch from high to low due to a spin flip on the dot [38].

#### D. Optical Measurements

Measurements of the Faraday rotation [2] originating from a pair of coupled electrons would allow us to distinguish between spin singlet and triplet [44]: In the singlet state ( $S = 0$ , no magnetic moment) there is no Faraday rotation, whereas in the triplet state ( $S = 1$ ) the

polarization of linearly polarized light is rotated slightly due to the presence of the magnetic moment. A single spin  $|\alpha\rangle$  can be measured either directly via Faraday rotation or by first entangling it with another spin  $|\uparrow\rangle$  and then applying the singlet/triplet-measurement. This entanglement is achieved by applying the gate defined in Sec. III C, resulting in either a triplet or singlet, depending on whether  $|\alpha\rangle$  was  $|\uparrow\rangle$  or  $|\downarrow\rangle$ . However, much more work is required to analyze the Faraday rotation (in particular to calculate the oscillator strength for such processes) in order to assess its efficiency for spin measurements.

## VI. QUANTUM COMMUNICATION WITH ENTANGLED ELECTRONS

A (pure) state of two particles (qubits) is called entangled, if it cannot be expressed as a tensor product of two single-particle states. Many tasks in quantum communication require maximally entangled states of two qubits (EPR pairs) such as the spin singlet [23]. Note that also the triplet  $|T_0\rangle$  is an entangled state, while the other two triplets  $|T_{\pm}\rangle$  are not. The quantum gate mechanism described in Sec. III C is one possibility for producing such entangled states (we call in general such a device an *entangler*, for which a number of realizations are conceivable). Here we discuss three experimental setups by which the entanglement of electrons can be detected via their charge in transport and noise measurements in mesoscopic nanostructures [9,55,56,43]. This investigation touches on fundamental issues such as the non-locality of quantum mechanics, especially for massive particles, and genuine two-particle Aharonov-Bohm effects which are fascinating topics in their own right. The main idea here is to exploit the unique relation between the symmetry of the orbital state and the spin state (for two electrons) which makes it possible to detect the spin state again via the charge (orbital) degrees of freedom of the electrons.

We should emphasize here that entanglement *per se* is rather the rule than the exception in condensed matter systems. For instance every ground state of a many-electron system is entangled simply by the antisymmetry requirement for the wave function. However, the key here is to have separate control over each specified particle which belongs to an entangled many-particle state.

In quantum optics, violations of Bell inequalities and quantum teleportation with photons have been investigated [57,58], while so far no corresponding experiments for electrons in a solid-state environment are reported.

### A. Adding Entangled Electrons to the Fermi Sea

When we consider the injection of entangled electrons into a Fermi sea, we must keep in mind that there is

always Coulomb interaction present with all the other electrons in the leads. So we need to analyze its effect on the entanglement [9,56]. Specifically, when we add an electron in state  $q$  to a Fermi sea (lead), the quasiparticle weight of that state will be renormalized by  $0 \leq z_q \leq 1$  (see below), i.e. some weight  $1 - z_q$  to find the electron in the original state  $q$  will be distributed among all the other electrons [9,56]. This rearrangement of the Fermi system due to the Coulomb interaction happens very quickly, on a timescale given by the inverse plasmon frequency. So, the question now is: how big is this renormalization? More precisely, when a triplet/singlet electron pair ( $t$  and  $s$  for short) is injected from an entangler into two leads 1 and 2, we obtain the state

$$|\psi_{\mathbf{n}\mathbf{n}'}^{t/s}\rangle = \frac{1}{\sqrt{2}} (a_{\mathbf{n}\uparrow}^{\dagger} a_{\mathbf{n}'\downarrow}^{\dagger} \pm a_{\mathbf{n}\downarrow}^{\dagger} a_{\mathbf{n}'\uparrow}^{\dagger}) |\psi_0\rangle, \quad (12)$$

with the filled Fermi sea  $|\psi_0\rangle$ ,  $\mathbf{n} = (\mathbf{q}, l)$ ,  $\mathbf{q}$  the momentum of an electron, and  $l$  the lead number. The operator  $a_{\mathbf{n}\sigma}^{\dagger}$  creates an electron in state  $\mathbf{n}$  with spin  $\sigma$ . The propagation of the triplet or singlet, interacting with all other electrons in the Fermi sea, can be described by the 2-particle Green's function  $G^{t/s}(\mathbf{12}, \mathbf{34}; t) = \langle \psi_{\mathbf{12}}^{t/s}, t | \psi_{\mathbf{34}}^{t/s} \rangle$ . If we prepare a triplet (singlet),  $G^{t/s}(\mathbf{12}, \mathbf{12}; t)$  is the amplitude of finding a triplet (singlet) after time  $t$ . Assuming sufficiently separated leads with negligible mutual interaction, we find [9,56]  $|G^{t/s}(\mathbf{12}, \mathbf{12}; t)| = z_F^2$ . For a spin-independent Hamiltonian with bare Coulomb interaction only and within RPA [51], the quasiparticle weight for a 2DEG is given by [9,56]  $z_F = 1 - r_s (1/2 + 1/\pi)$ , in leading order of the interaction parameter  $r_s = 1/k_F a_B$ , where  $a_B = \epsilon_0 \hbar^2 / m e^2$  is the Bohr radius and  $k_F$  the Fermi wavevector. In a GaAs 2DEG we have  $a_B = 10.3$  nm and  $r_s = 0.614$ , and thus we obtain  $z_F = 0.665$ . Therefore, we conclude that the entanglement of a pair of electrons injected into a Fermi liquid will be reduced but there is still a finite probability left to preserve the entangled state. This holds provided the spin-scattering effects are small. That this is indeed the case in GaAs 2DEGs is supported by experiments [2] where the electron spin has been transported phase-coherently over distances of up to  $100 \mu\text{m}$  [2].

### B. Noise of Entangled Electrons

It has been known [59,60] for quite some time that bosons such as photons show “bunching” behavior when measuring the correlations between particles (“noise”) in an incoming particle current. More recently, the opposite behavior for fermions, “antibunching”, was expected theoretically [61–63] and found experimentally [64], in particular for electrons. However, as we have pointed out recently [9] the noise of electrons in current-carrying wires is not sensitive to the symmetry of the total wave function but only to the symmetry of the *orbital* part of it, at least if no spin-scattering processes are present.

Thus, if we now consider a two-electron state, we expect antibunching for the triplet states, since they have an antisymmetric orbital wave function, whereas the orbital wave function associated with the spin singlet state is symmetric, and so we expect a bunching behavior. This leads to an observable decrease or increase in noise for electrons, depending on their common spin state, as we shall discuss next [56].

We assume that an entangler generates pairs of entangled electrons which are then injected into lead 1 and 2, one electron each, as shown in Fig. 4. A beam splitter is inserted in order to create two-particle interference effects in the sense that there is an equal probability amplitude for incoming electrons (from lead 1 or 2) to leave into lead 3 or 4 (note that the electrons in a Fermi liquid wire hardly interact with each other; the role of the beam splitter is thus to simulate direct and exchange Coulomb processes). The quantity of interest is then the noise, i.e. the current-current correlations, measured in leads 3 and/or 4.

The amplitude of recovering a singlet or triplet state after injecting it into an interacting Fermi sea is reduced by a factor of  $z_F^{-2} \approx 2$  (see Sec. VI A). Except for this renormalization, the entanglement of the singlet or triplet state is not affected by the interacting electrons in the filled Fermi sea. Thus we can now calculate transport quantities using the standard scattering theory for non-interacting quasiparticles in a Fermi liquid. We consider the entangled incident states  $|\pm\rangle \equiv |\psi_{12}^{t/s}\rangle$  with one electron per lead and the quantum numbers  $\mathbf{n} = (\varepsilon_n, n)$ , where  $\varepsilon_n$  is the energy of the electron. Considering a multiterminal conductor with density of states  $\nu$ , we assume that the leads consist of only one quantum channel; the generalization to several channels is straightforward. The (unpolarized) current operator for lead  $\alpha$  can be written as [61]

$$I_\alpha(t) = \frac{e}{h\nu} \sum_{\sigma \varepsilon \varepsilon'} [a_{\alpha\sigma}^\dagger(\varepsilon)a_{\alpha\sigma}(\varepsilon') - b_{\alpha\sigma}^\dagger(\varepsilon)b_{\alpha\sigma}(\varepsilon')] e^{i(\varepsilon - \varepsilon')t/\hbar}, \quad (13)$$

where  $a_{\alpha\sigma}^\dagger(\varepsilon)$  creates an incoming electron with spin  $\sigma$  and energy  $\varepsilon$  in the lead  $\alpha$ . The operators  $b_{\alpha\sigma}(\varepsilon)$  for the outgoing electrons are given by  $b_{\alpha\sigma}(\varepsilon) = \sum_\beta s_{\alpha\beta} a_{\beta\sigma}(\varepsilon)$  with the scattering matrix  $s_{\alpha\beta}$ , which is assumed to be spin- and energy-independent. The average currents in the leads,  $|\langle I_\alpha \rangle| = e/h\nu$ , are not sensitive to the orbital symmetry of the wavefunction. The spectral densities of the fluctuations  $\delta I_\alpha = I_\alpha - \langle I_\alpha \rangle$  between the leads  $\alpha$  and  $\beta$  are

$$S_{\alpha\beta}(\omega) = \lim_{T \rightarrow \infty} \frac{h\nu}{T} \int_0^T dt e^{i\omega t} \text{Re}(\pm |\delta I_\alpha(t) \delta I_\beta(0)| \pm), \quad (14)$$

which are now evaluated with the scattering matrix for the beamsplitter (Fig. 4) with the reflection and transmission amplitudes  $r$  and  $t$ , thus  $s_{31} = s_{42} = r$ , and  $s_{41} =$

$s_{32} = t$  and no backscattering, so  $s_{12} = s_{34} = s_{\alpha\alpha} = 0$ . We obtain for the noise at zero frequency [56]

$$S_{33} = S_{44} = -S_{34} = 2 \frac{e^2}{h\nu} T(1-T)(1 \mp \delta_{\varepsilon_1 \varepsilon_2}). \quad (15)$$

Here, the minus (plus) sign refers to the spin triplet (singlet) and  $T = |t|^2$  is the transmission coefficient of the beam splitter. If two electrons with the same energies,  $\varepsilon_1 = \varepsilon_2$ , in the singlet state are injected into the leads 1 and 2, the shot noise is enhanced by a factor of two compared to the value for uncorrelated particles [61,65],  $2e^2T(1-T)/h\nu$ . This amplification of the noise arises from *bunching* of the electrons due to their symmetric orbital wavefunction, such that the electrons preferably appear in the same outgoing leads. If the electron pairs are injected as a triplet, an *antibunching* effect appears, completely suppressing the noise, i.e.  $S(\omega=0) = 0$ . We stress that the sign of cross-correlations does not carry any signature of statistics, e.g. here the different signs of  $S_{34}$  and  $S_{33} = S_{44}$  [Eq. (15)] merely reflect current conservation and absence of backscattering. Since the bunching effect appears only for a state with a symmetric orbital wave function, which is not the case for unentangled electron states, measuring noise enhancement in the outgoing arms of the beamsplitter provides unique evidence for entanglement [56].

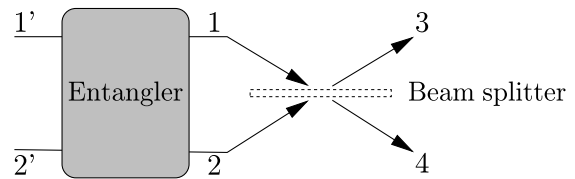


FIG. 4. The proposed setup for measuring noise of entangled electrons. The entangler takes uncorrelated electrons from the Fermi leads 1' and 2'. Pairs of entangled electrons (singlet or triplet) are produced in the entangler and then injected into the leads 1 and 2, one electron per lead. The current of these two leads are then mixed with a beam splitter (to induce scattering interference) and the resulting noise is then measured in lead 3 and 4: no noise (antibunching) for triplets, whereas we get enhanced noise (bunching) for singlets (i.e. EPR pairs).

### C. Spin-dependent Current through a Double Dot—Probing Entanglement

We turn now to a setup by which the entanglement of two electrons in a double-dot can be measured through current and noise [55]. For this we consider a double-dot which is weakly coupled, with tunneling amplitude  $\Gamma$ , to in-and outgoing leads at chemical potentials  $\mu_{1,2}$ . As shown in Fig. 5, the dots are put in parallel in contrast to the standard series connection. We work in the Coulomb blockade regime [24] where the charge on the dots is quantized and in the cotunneling regime [53,66],

with  $U > |\mu_1 \pm \mu_2| > J > k_B T, 2\pi\nu\Gamma^2$ , where  $U$  is the single-dot charging energy,  $\nu$  the lead density of states, and  $J$  the exchange coupling (see Sec. III). The cotunneling current involves a coherent virtual process where an electron tunnels from a dot to, say, lead 2 and then a second electron tunnels from lead 1 to this dot. Assuming  $|\mu_1 - \mu_2| > J$ , elastic as well as inelastic cotunneling occurs. Further,  $\Gamma$  is assumed to be sufficiently weak so that the double-dot will return to its equilibrium state before the next electron passes through. Since an electron can either pass through the upper or lower dot, a closed loop is formed by these two paths, and in the presence of a magnetic flux the upper and the lower paths collect a phase difference given by the Aharonov-Bohm phase  $\phi = ABe/\hbar$  (with  $A$  being the loop area), thus leading to interference effects. If the two electrons on the double-dot are in the *singlet state*, then the tunneling current acquires an additional phase of  $\pi$  (see below and Fig. 5) leading to a sign reversal of the coherent contribution compared to that for triplets. Explicitly, we find for the cotunneling current [55]

$$I = e\pi\nu^2\Gamma^4 \frac{\mu_1 - \mu_2}{\mu_1\mu_2} (2 \pm \cos\phi), \quad (16)$$

and for the shot noise power  $S(0) = -e|I|$ , where the upper sign refers to the triplet states in the double-dot and the lower sign to the singlet state.

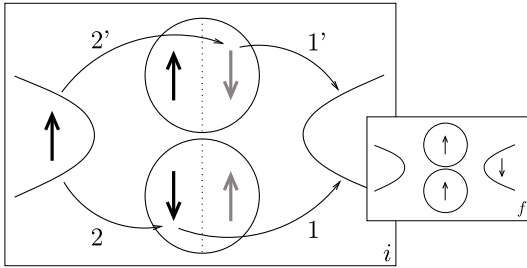


FIG. 5. Two coupled quantum dots with tunnel contacts to in- and outgoing leads to probe the entanglement on the dot (see text). The large box shows an initial state  $i$  with one spin-up electron in the left lead and two electrons on the double dot in state  $(|\uparrow\downarrow\rangle \pm |\downarrow\uparrow\rangle)/\sqrt{2}$ , where the first term is drawn in black in the left part of the dots and the second term in gray on the right. After the tunneling processes 1, 2 or 1', 2', the final state  $f$  is reached, where a spin-down electron is in the right lead and the state on the dots is  $|T_+\rangle = |\uparrow\uparrow\rangle$ , as shown in the small box.

Eq. (16) can be reproduced, up to a prefactor, by the following heuristic argument. Consider the two spins on the double dot to be in the singlet state  $|S\rangle = (|\uparrow\downarrow\rangle - |\downarrow\uparrow\rangle)/\sqrt{2}$  or in a triplet state, say,  $|T_0\rangle = (|\uparrow\downarrow\rangle + |\downarrow\uparrow\rangle)/\sqrt{2}$ . These superpositions are illustrated in Fig. 5 by drawing the first term in black in the left part of the dots and the second term in gray on the right. We consider the contribution  $I_{T_+}$  to the current, where we start with one spin-up electron in the left lead and end with

a spin-down electron in the right lead and the triplet state  $|T_+\rangle$  on the double dot (see inset of Fig. 5). For this process, either a spin-down electron tunnels first (1) from the lower dot into the right lead and then (2) the spin-up electron from the left lead tunnels into the lower dot. Or the upper dot participates via (1') and (2'), but now the state  $|\downarrow\uparrow\rangle$  is involved, thus if the initial state on the double dot is a singlet, the transition amplitudes for upper and lower path acquire opposite signs, whereas there is no sign change if we started out from a triplet (as shown for  $|T_0\rangle$  in Fig. 5). Therefore, we can write the transition amplitudes  $A_{21} = |A_{21}|e^{i\phi/2} \propto \Gamma^2$  for the lower path and  $A_{2'1'} = \pm|A_{21}|e^{-i\phi/2}$  for the upper path, where the upper/lower sign stands for a triplet/singlet initial state on the double-dot. This leads to a total transition amplitude of  $A_{fi} = A_{21} + A_{2'1'}$ , and a current  $I_{T_+} \propto e|A_{fi}|^2 = 2e|A_{21}|^2(1 \pm \cos\phi)$ . Note that the transition  $|S\rangle \rightarrow |T_+\rangle$  is inelastic whereas  $|T_0\rangle \rightarrow |T_+\rangle$  is not. For an initial singlet state on the double-dot, the other inelastic processes  $|S\rangle \rightarrow |T_0\rangle, |T_-\rangle$  also yield a current proportional to  $1 - \cos\phi$ , while the current from the elastic process  $|S\rangle \rightarrow |S\rangle$  is proportional to  $1 + \cos\phi$ . Similarly, starting with a triplet, the sign of the  $\cos\phi$  term is negative for an inelastic process, while it is positive for an elastic one. Note that there is only one inelastic process  $|T\rangle \rightarrow |S\rangle$ , whereas there are more elastic processes allowed for  $|T\rangle \rightarrow |T\rangle$ . The total current is obtained by summing over all terms, yielding  $I = \sum_f I_f \propto e\Gamma^4(2 \pm \cos\phi)$ , where the upper sign stands for an initial triplet state and the lower sign for a singlet, in agreement with Eq. (16). We finally emphasize that for the singlet  $|S\rangle$  and for the triplet  $|T_0\rangle$  the double-dot state is entangled, i.e. a correlated two-particle state, and thus the proposed setup probes a genuine two-particle interference effect via the Aharonov-Bohm oscillations in the current (noise). Note also that we can continuously transmute the statistics from fermionic to bosonic (like for anyons): the symmetric orbital part of  $|S\rangle$  goes into an antisymmetric one at half a flux quantum, and vice versa for  $|T_0\rangle$ .

We have evaluated the noise also for finite frequencies [55], and found that again  $S(\omega) \propto (2 \pm \cos\phi)$ , and, moreover, that the odd part of  $S(\omega)$  leads to slowly decaying oscillations of the noise in real time,  $S(t) \propto \sin(\mu t)/\mu t$ ,  $\mu = (\mu_1 + \mu_2)/2$ , which can be ascribed to a charge imbalance on the double dot during an uncertainty time  $\mu^{-1}$ .

We finally note that the three triplets can be further distinguished by an orientationally inhomogeneous magnetic field which results in a spin-Berry phase [67,55] that leads to left, right or no phase-shift in the Aharonov-Bohm oscillations of the current (noise).

## D. Double Dot with Superconducting Leads

We have considered a further scenario of double-dots [43], where the dots are aligned in parallel between the leads, as in Sec. VI C, but now no direct coupling is assumed between them. However, they are coupled with a tunneling amplitude  $\Gamma$  to two superconducting leads. The s-wave superconductor favors an entangled singlet-state on the dots (like in a Cooper pair) and further provides a mechanism for detecting the spin state via the Josephson current. It turns out that in leading order  $\propto \Gamma^4$  the spin coupling is again described by a Heisenberg Hamiltonian [43]

$$H_{\text{eff}} \approx J(1 + \cos \varphi) \left( \mathbf{S}_a \cdot \mathbf{S}_b - \frac{1}{4} \right), \quad (17)$$

where  $J \approx 2\Gamma^2/\epsilon$ , and the energy of the dot is  $\epsilon$  below the lead Fermi energy. Here,  $\varphi$  is the average phase difference across the superconductor–double-dot–superconductor (S-DD-S) junction. We can modify the exchange coupling between the spins by tuning the external control parameters  $\Gamma$  and  $\varphi$ . Thus, we have presented here another implementation of a two-qubit quantum gate (see Sec. III) or an “entangler” for EPR transport (see Sec. VI B). Furthermore, the spin state on the dot can be probed if the superconducting leads are joined with one additional (ordinary) Josephson junction with coupling  $J'$  and phase difference  $\theta$  into a SQUID-ring. The supercurrent  $I_S$  through this ring is given by [43]

$$I_S/I_J = \begin{cases} \sin(\theta - 2\pi f) + (J'/J) \sin \theta, & \text{singlet,} \\ (J'/J) \sin \theta, & \text{triplets,} \end{cases} \quad (18)$$

where  $I_J = 2eJ/\hbar$ . Measurement of the spin- and flux-dependent critical current  $I_c = \max_{\theta} \{|I_S|\}$  probes the spin state of the double dot. This is realized by biasing the system with a dc current  $I$  until a finite voltage  $V$  appears for  $|I| > I_c$  [43].

## VII. CONCLUSIONS

We have described a concept for a quantum computer based on electron spins in quantum-confined nanostructures, in particular quantum dots, and presented theoretical proposals for manipulation, coupling and detection of spins in such structures. We have discussed the requirements for initialization, read-in, gate operations, read-out, coherence, switching times and precision and their actual realization. By putting it all together, we have illustrated how a scalable, all-electronically controlled quantum computer can be envisioned.

We have shown that there is a fruitful link between mesoscopic transport phenomena and quantum communication that is based on production, detection and transport of electronic EPR pairs. We have proposed and analyzed a variety of experimental setups which would

probe novel spin-based phenomena in open and closed mesoscopic nanostructures. The involved physics, which is based on strong correlations and spin phase-coherence of electrons, is of fundamental interest in its own right—quite apart from future applications.

Finally, by implementing the ideas proposed here, experimental evidence could be gained to demonstrate controlled entanglement and coherence of electron spins in nanostructures. This would be a first step in showing that the proposed scheme of spin-based qubits is indeed suitable for quantum computing and quantum communication.

## ACKNOWLEDGMENTS

We would like to thank K. Ensslin, E.V. Sukhorukov, and P. Recher for many discussions. This work has been supported by the Swiss National Science Foundation.

- 
- [1] G. Prinz, *Phys. Today* **45**(4), 58 (1995); G. A. Prinz, *Science* **282**, 1660 (1998).
  - [2] J.M. Kikkawa, I.P. Smorchkova, N. Samarth, and D.D. Awschalom, *Science* **277**, 1284 (1997); J.M. Kikkawa and D.D. Awschalom, *Phys. Rev. Lett.* **80**, 4313 (1998); D.D. Awschalom and J.M. Kikkawa, *Phys. Today* **52**(6), 33 (1999).
  - [3] R. Fiederling *et al.*, *Nature* **402**, 787 (1999).
  - [4] Y. Ohno *et al.*, *Nature* **402**, 790 (1999).
  - [5] F.G. Monzon and M.L. Roukes, *J. Magn. Magn. Mater.* **198**, 632 (1999).
  - [6] S. Lüscher *et al.*, cond-mat/0002226.
  - [7] D. Loss and D.P. DiVincenzo, *Phys. Rev. A* **57**, 120 (1998); cond-mat/9701055.
  - [8] A. Steane, *Rep. Prog. Phys.* **61**, 117 (1998).
  - [9] D.P. DiVincenzo and D. Loss, *J. Magn. Magn. Mater.* **200**, 202 (1999); cond-mat/9901137.
  - [10] C. H. Bennett and D. P. DiVincenzo, *Nature* **404**, 247 (2000).
  - [11] D.P. DiVincenzo, G. Burkard, D. Loss, and E. Sukhorukov, in *Quantum Mesoscopic Phenomena and Mesoscopic Devices in Microelectronics*, eds. I.O. Kulik and R. Ellialtoglu (NATO ASI, Turkey, June 13-25, 1999); see cond-mat/99112445.
  - [12] P.W. Shor, in *Proc. 35th Symposium on the Foundations of Computer Science*, (IEEE Computer Society Press), 124 (1994).
  - [13] L.K. Grover, *Phys. Rev. Lett.* **79**, 325 (1997).
  - [14] J.I. Cirac and P. Zoller, *Phys. Rev. Lett.* **74**, 4091 (1995); C. Monroe *et al.*, *ibid.* **75**, 4714 (1995).
  - [15] Q.A. Turchette *et al.*, *Phys. Rev. Lett.* **75**, 4710 (1995).
  - [16] D. Cory, A. Fahmy, and T. Havel, *Proc. Nat. Acad. Sci. U.S.A.* **94**, 1634 (1997); N. A. Gershenfeld and I. L. Chuang, *Science* **275**, 350 (1997).

- [17] B. Kane, *Nature* **393**, 133 (1998).
- [18] A. Shnirman, G. Schön, and Z. Hermon, *Phys. Rev. Lett.* **79**, 2371 (1997).
- [19] D.V. Averin, *Solid State Commun.* **105**, 659 (1998).
- [20] L.B. Ioffe *et al.*, *Nature* **398**, 679 (1999).
- [21] T.P. Orlando *et al.*, *Phys. Rev. B* **60**, 15398 (1999).
- [22] C. H. Bennett *et al.*, *Phys. Rev. Lett.* **70**, 1895 (1993).
- [23] C. H. Bennett and G. Brassard, in *Proceedings of the IEEE International Conference on Computers, Systems and Signal Processing*, Bangalore, India (IEEE, NY, 1984), p. 175.
- [24] L. P. Kouwenhoven *et al.*, *Proceedings of the ASI on Mesoscopic Electron Transport*, eds. L.L. Sohn, L.P. Kouwenhoven, and G. Schön (Kluwer, 1997).
- [25] S. Tarucha *et al.*, *Phys. Rev. Lett.* **77**, 3613 (1996).
- [26] F.R. Waugh *et al.*, *Phys. Rev. Lett.* **75**, 705 (1995); C. Livermore *et al.*, *Science* **274**, 1332 (1996).
- [27] T. H. Oosterkamp *et al.*, *Phys. Rev. Lett.* **80**, 4951 (1998).
- [28] R.H. Blick *et al.*, *Phys. Rev. Lett.* **80**, 4032 (1998); *ibid.* **81**, 689 (1998). T.H. Oosterkamp *et al.*, *Nature* **395**, 873 (1998); I.J. Maasilta and V.J. Goldman, *Phys. Rev. Lett.* **84**, 1776 (2000).
- [29] J.A. Gupta, D.D. Awschalom, X. Peng, and A.P. Alivisatos, *Phys. Rev. B* **59**, R10421 (1999).
- [30] A. V. Khaetskii and Y. V. Nazarov, *Phys. Rev. B* **61**, 12639 (2000); *cond-mat/00035513*.
- [31] G. Burkard, D. Loss, and D. P. DiVincenzo, *Phys. Rev. B* **59**, 2070 (1999).
- [32] A. Imamoglu *et al.*, *Phys. Rev. Lett.* **83**, 4204 (1999).
- [33] G. Burkard, D. Loss, D.P. DiVincenzo, and J.A. Smolin, *Phys. Rev. B* **60**, 11404 (1999).
- [34] P.W. Shor, *Phys. Rev. A* **52**, R2493 (1995); A.M. Steane, *Phys. Rev. Lett.* **77**, 793 (1996); D.P. DiVincenzo and P.W. Shor, *ibid.* **77**, 3260 (1996); E. Knill and R. Laflamme, *Phys. Rev. A* **55**, 900 (1997); D. Gottesman, *ibid.* **54**, 1862 (1996); E. Dennis, *quant-ph/9905027*.
- [35] L. Kouwenhoven and C. Marcus, private communication.
- [36] M. Dohers *et al.*, *Phys. Rev. Lett.* **61**, 1650 (1988).
- [37] D. C. Dixon, K. R. Wald, P. L. McEuen, and M. R. Melloch, *Phys. Rev. B* **56**, 4743 (1997).
- [38] P. Recher, E.V. Sukhorukov, and D. Loss, *cond-mat/0003089*.
- [39] R. Shankar, *Principles of Quantum Mechanics*, Ch. 14, Plenum Press, New York, 1994.
- [40] D.P. DiVincenzo, *Phys. Rev. A* **51**, 1015 (1995).
- [41] A. Barenco *et al.*, *Phys. Rev. A* **52**, 3457 (1995).
- [42] R. Vrijen *et al.*, *quant-ph/9905096*.
- [43] M.-S. Choi, C. Bruder, and D. Loss, *cond-mat/0001011*.
- [44] G. Burkard, G. Seelig, and D. Loss, to be published in *Phys. Rev. B*, July 2000; *cond-mat/9910105*.
- [45] R. J. Luyken *et al.*, preprint.
- [46] D. G. Austing *et al.*, *Physica B* **249-251**, 206 (1998).
- [47] E.L. Ivchenko, A.A. Kiselev, and M. Willander, *Solid State Comm.* **102**, 375 (1997).
- [48] K. Ensslin, private communication.
- [49] A. Peres, *Quantum Theory: Concepts and Methods* (Kluwer, Dordrecht, 1993).
- [50] M. Devoret, D. Estève, and Ch. Urbina, *Nature (London)* **360**, 547 (1992).
- [51] G. D. Mahan, *Many Particle Physics*, 2nd Ed. (Plenum, New York, 1993).
- [52] L.P. Kouwenhoven, G. Schön, and L. L. Sohn, *Mesoscopic Electron Transport*, NATO ASI Series E: Applied Sciences-Vol. 345 Kluwer Academic Publishers, 1997.
- [53] D. V. Averin and Yu. V. Nazarov, in *Single Charge Tunneling*, eds. H. Grabert, M. H. Devoret, NATO ASI Series B: Physics Vol. 294, Plenum Press, New York, 1992.
- [54] M. Ciorga *et al.*, *cond-mat/9912446*.
- [55] D. Loss and E.V. Sukhorukov, *Phys. Rev. Lett.* **84**, 1035 (2000).
- [56] G. Burkard, D. Loss, and E.V. Sukhorukov, to be published in *Phys. Rev. B*, June 2000; *cond-mat/9906071*.
- [57] A. Aspect, J. Dalibard, and G. Roger, *Phys. Rev. Lett.* **49**, 1804 (1982); W. Tittel, J. Brendel, H. Zbinden, and N. Gisin, *Phys. Rev. Lett.* **81**, 3563 (1998).
- [58] D. Bouwmeester *et al.*, *Nature* **390**, 575 (1997); D. Boschi *et al.*, *Phys. Rev. Lett.* **80**, 1121 (1998).
- [59] R. Loudon, *Phys. Rev. A* **58**, 4904 (1998).
- [60] R. Hanbury Brown and R. Q. Twiss, *Nature (London)* **177**, 27 (1956).
- [61] M. Büttiker, *Phys. Rev. Lett.* **65**, 2901 (1990); *Phys. Rev. B* **46**, 12485 (1992).
- [62] T. Martin and R. Landauer, *Phys. Rev. B* **45**, 1742 (1992).
- [63] E.V. Sukhorukov and D. Loss, *Phys. Rev. B* **59**, 13054 (1999).
- [64] R. C. Liu, B. Odom, Y. Yamamoto, and S. Tarucha, *Nature* **391**, 263 (1998); M. Henny *et al.*, *Science* **284**, 296 (1999); W. D. Oliver *et al.*, *ibid.*, 299 (1999).
- [65] V. A. Khlus, *Zh. Eksp. Teor. Fiz.* **93**, 2179 (1987).
- [66] J. König, H. Schoeller, and G. Schön, *Phys. Rev. Lett.* **78**, 4482 (1997).
- [67] D. Loss and P. Goldbart, *Phys. Rev. B* **45**, 13544 (1992).